Dalton Transactions

Accepted Manuscript

ROYAL SOCIETY OF CHEMISTRY

www.rsc.org/dalton

Journal Name

RSCPublishing

ARTICLE

A Facile Exfoliation–Crystal Growth Route to Multicomponent Ag_2CO_3/Ag–Ti_5NbO_{14} Nanohybrids with Improved Visible Light Photocatalytic Activity

Cite this: DOI: 10.1039/x0xx00000x

Received 00th January 2012,
Accepted 00th January 2012

DOI: 10.1039/x0xx00000x

www.rsc.org/

Suhye Park,[a,†] Jang Mee Lee,[a,†] Yun Kyung Jo,[a] In Young Kim,[a] and Seong-Ju Hwang*[,a]

Multicomponent Ag_2CO_3/Ag–layered Ti_5NbO_{14} nanohybrids are synthesized by the crystal growth of silver carbonate on the surface of exfoliated layered titanoniobate 2D nanosheet. In the obtained nanohybrids, the spherical Ag_2CO_3 nanoparticles with the size of 5–10 nm are immobilized on the surface of the titanoniobate nanosheets with the partial formation of neutral Ag metal caused by an electron transfer from anionic titanoniobate nanosheets to silver cations. An electronic coupling between Ag_2CO_3/Ag and Ti_5NbO_{14} nanosheet leads to a remarkable enhancement of visible light absorption and a significant depression of electron–hole recombination. The present Ag_2CO_3/Ag–layered Ti_5NbO_{14} nanohybrids show much higher visible light photocatalytic activity than do unhybridized Ag_2CO_3, underscoring the beneficial effect of hybridization with metal oxide nanosheets on the photocatalytic activity of silver oxosalt. Before and after the photoreaction, the crystal structure and crystal morphology of the Ag_2CO_3/Ag–layered Ti_5NbO_{14} nanohybrids remain unchanged, highlighting the excellent photostability of these materials. All the present experimental findings clearly demonstrate the usefulness of the exfoliation–crystal growth method in exploring novel efficient visible light active photocatalysts.

Introduction

Semiconductor-assisted photocatalytic reactions such as water photosplitting and the photodegradation of organic pollutants receive special attention because of their usefulness as economic and eco-friendly options for the depletion of fossil fuel and the deepening threat of environmental pollution.[1–11] There are several factors to be considered in designing efficient photocatalysts such as an optimized band structure for the harnessing of visible light, an enhanced transport of photogenerated electrons and holes, a promoted reaction kinetics on surface sites, etc.[12–17] Since most of metal oxide-based semiconductors have wide bandgap energy and thus cannot absorb visible light, the control of the bandgap energy of these materials is indispensible for the development of visible light active photocatalysts.[18–24] One of the most useful methods to provide metal oxide semiconductor with visible light harvesting ability is to hybridize with narrow bandgap semiconductors.[12,15,22,25,26] Taking into account the very thin thickness and wide surface area of 2D nanosheets, the exfoliated nanosheets of semiconducting inorganic solids are one of the most useful building blocks for the maximization of an electronic coupling between the hybridized components.[25,27–31] The house-of-cards-type stacking of the exfoliated nanosheets upon hybridization leads to the formation of highly porous structure, which is also beneficial in enhancing the reaction kinetics occurring on surface sites.[18,32] In fact, an electrostatically-derived hybridization between anionic metal oxide nanosheets and cationic narrow bandgap semiconductor nanoclusters is fairly useful in exploring novel visible light active photocatalysts.[12,18,22] Recently silver oxosalts like Ag_3PO_4 attract intense research activity because of their excellent photocatalyst performance under visible light irradiation.[33–35] The hybridization of silver oxosalts with metal oxide 2D nanosheets is expected to further improve their photocatalytic activity via the increase of the lifetime of electrons and holes. However, a difficulty in preparing cationic silver oxosalt nanoclusters frustrates the application of electrostatically-derived self-assembly strategy for coupling silver oxosalt with negatively-charged metal oxide nanosheets. The direct crystal growth of silver oxosalts on the surface of metal oxide nanosheets is supposed to provide an alternative synthetic route to Ag oxosalt–metal oxide nanohybrids with visible light photocatalytic activity. This synthetic strategy possesses another merit of the tailoring the chemical composition of the resulting nanohybrid material. In one instance, the partial reduction of silver cations during the crystal growth of silver oxosalt gives rise to the formation of multicomponent silver oxosalt/silver–metal oxide nanohybrids. The presence of highly conductive silver metal component would facilitate an electron transfer between silver oxosalts and metal oxide nanosheets, leading to the suppression of electron–hole recombination. Although there are several examples of Ag_3PO_4-containing hybrid materials,[36,37] we are

unaware of the crystal growth-derived synthesis of multicomponent silver carbonate/silver–metal oxide nanohybrids using exfoliated metal oxide nanosheets.

In the present study, a facile synthetic route to mesoporous Ag_2CO_3/Ag–layered Ti_5NbO_{14} nanohybrids is developed by the direct crystal growth of silver carbonate/silver on the surface of the exfoliated titanoniobate nanosheets. To probe the effect of chemical composition on the physicochemical properties of the resulting nanohybrids, the Ag_2CO_3/Ti_5NbO_{14} ratios of 0.5 and 1 are applied. The obtained Ag_2CO_3/Ag–Ti_5NbO_{14} nanohybrids are denoted as **AT1** and **AT2**, respectively. The crystal structure, optical property, and pore structure of the obtained nanohybrids are characterized with powder X-ray diffraction (XRD), electron microscopy, diffuse reflectance UV–vis and photoluminescence (PL) spectroscopy, and N_2 adsorption–desorption isotherm measurement, respectively. The effects of hybridization on the electronic and local crystal structures of hybridized silver species and titanoniobate nanosheets are examined with X-ray absorption spectroscopy (XAS) and X-ray photoelectron spectroscopy (XPS). The photocatalytic activity of the obtained nanohybrids is investigated for the photodegradation of organic molecules under the illumination of visible light.

Results and discussion

Powder XRD Analysis.

The powder XRD patterns of the pristine $K_3Ti_5NbO_{14}$ compound and its protonated and exfoliated derivatives are presented in Fig. 1. Upon the reaction with HCl, the (*h00*) peak of the pristine potassium titanoniobate is slightly replaced toward higher angle side, indicating the minute decrease of basal spacing. The observed basal contraction indicates the replacement of bigger K^+ ions with smaller H^+ ions. After the reaction of the protonated titanoniobate with tetrabutylammonium (TBA^+) cations, the colloidal suspension of exfoliated $Ti_5NbO_{14}^-$ nanosheets is obtained. After the restoration of the obtained colloidal suspension via freeze-drying, a series of (*h00*) reflections appear at low angle region, indicating the formation of TBA-intercalation compound.

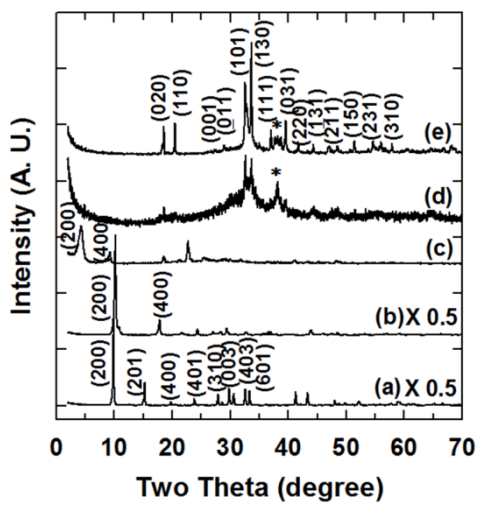

Fig. 1 Powder XRD patterns of (a) the pristine $K_3Ti_5NbO_{14}$, (b) the protonated $H_3Ti_5NbO_{14}$, (c) the exfoliated Ti_5NbO_{14} nanosheets, and the Ag_2CO_3/Ag–Ti_5NbO_{14} nanohybrids of (d) **AT1** and (e) **AT2**. The asterisk denotes the (111) Bragg reflection of Ag metal.

Both of the present **AT** nanohybrids display the XRD peaks of Ag_2CO_3, indicating the formation of silver carbonate. The reaction between silver cations and dissolved carbonate anions in basic solution is responsible for the synthesis of silver carbonate, as illustrated in Fig. 2. In addition, weak XRD peak of Ag metal phase is observed in the present patterns, indicating the formation of silver metal due to the partial reduction of Ag^+ ions during the hybridization process.

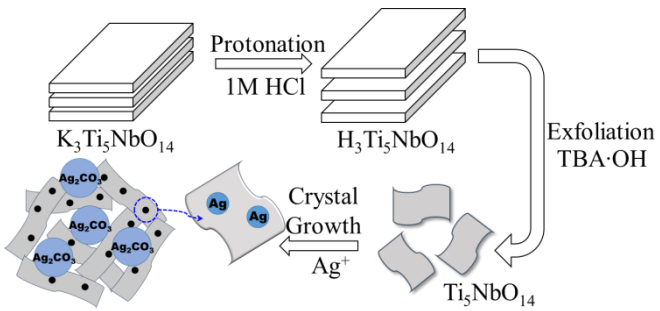

Fig. 2 Schematic diagram for crystal growth route to Ag_2CO_3/Ag–Ti_5NbO_{14} nanohybrid.

In contrast to the silver species, no Bragg reflections of titanoniobate phase appear in the present XRD patterns of the **AT** nanohybrids, suggesting the homogeneous dispersion of nanosheets in these materials without any phase segregation. A similar phenomenon is frequently observed for many graphene nanosheet-based hybrid materials.[38]

FE-SEM/EDS and HR-TEM Analyses.

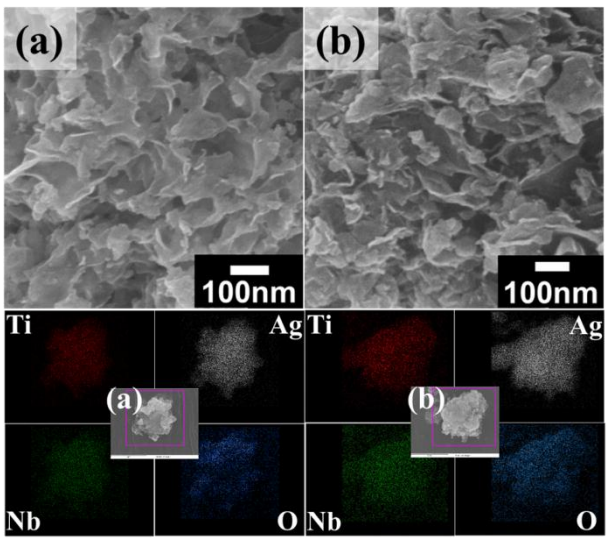

Fig. 3 (Top) FE-SEM images and (bottom) elemental maps and (center) FE-SEM images of (a) **AT1** and (b) **AT2**.

The crystal morphology of the present **AT** nanohybrids is studied with field emission-scanning electron microscopy (FE-SEM). As presented in the top panel of Fig. 3, the nanoparticles of silver carbonate appear on the surface of

titanoniobate nanosheets, confirming the hybridization between these species. Also both of the **AT** materials commonly show mesoporous morphology, which is formed by the house-of-cards-type stacking structure of the nanosheet crystallites. This finding demonstrates the usefulness of the restacking of 2D nanosheets in the formation of highly porous structure. As illustrated in the bottom panel of Fig. 3, energy dispersive spectrometry (EDS)–elemental mapping analysis confirms the hybridization between silver species and titanoniobate nanosheets. Regardless of the Ag/Ti ratios, all of the Ag, Ti, Nb, and O elements are homogeneously distributed in entire parts of the **AT** nanohybrids, clearly demonstrating the uniform hybridization between silver species and titanoniobate nanosheets. This result indicates that, despite no observation of the XRD peaks of titanoniobate, the Ti_5NbO_{14} nanosheets are surely present in all the present nanohybrid materials. According to the EDS analysis, the Ag/Ti ratio of the present Ag_2CO_3/Ag–Ti_5NbO_{14} nanohybrids is determined to be 1.7 and 2.6 for **AT1** and **AT2**, respectively.

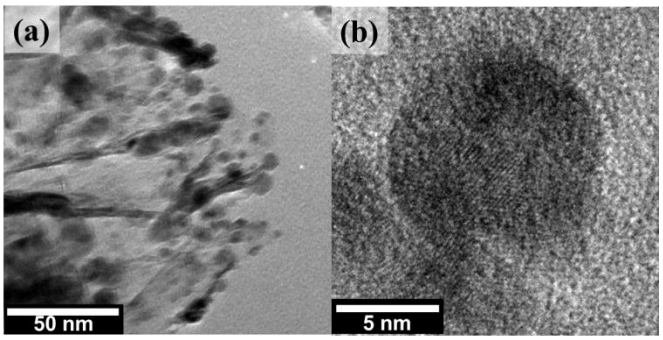

Fig. 4. HR-TEM images of the **AT2** nanohybrid with (a) low and (b) high magnification ratio.

The composite formation between silver species and titanoniobate nanosheets is further confirmed by high resolution-transmission electron microscopy (HR-TEM) analysis. The HR-TEM image of Fig. 4 exhibits the stabilization of silver carbonate crystal on the surface of very thin titanoniobate nanosheets in the **AT2** nanohybrid. The particle size of silver carbonate is found to be ~5–10 nm, confirming the usefulness of metal oxide nanosheets as a support to stabilize nanocrystalline silver oxosalt.

N_2 Adsorption–Desorption Isotherm Analysis.

Fig. 5 represents the N_2 adsorption–desorption isotherms of the self-assembled **AT** nanohybrids. Almost identical isotherm behaviors occur for both the present nanohybrids. The observed isotherms can be classified as the Brunauer–Deming–Deming–Teller (BDDT) type IV shape and H3-type hysteresis loop in the IUPAC classification,[39] indicating the formation of mesopores corresponding to open slit-shaped capillaries with very wide bodies and narrow short necks. As evidenced by the FE-SEM analysis (Fig. 3), the formation of mesopores is attributable to the house-of-cards type stacking structure of sheet-like crystallites.[40] According to the fitting analysis with the Brunauer–Emmett–Teller (BET) equation, the surface areas of the present nanohybrids are determined as 58 and 41 m^2g^{-1} for **AT1** and **AT2**, respectively, which is much greater than that of the pristine titanoniobate (~1 m^2g^{-1}). This finding provides clear evidence for the usefulness of exfoliated nanosheets in forming the highly porous structure with expanded surface area. An increase of Ag content in the present **AT** nanohybrids causes the decrease of surface area, which can be interpreted as a result of the pore blocking by hybridized silver carbonate.

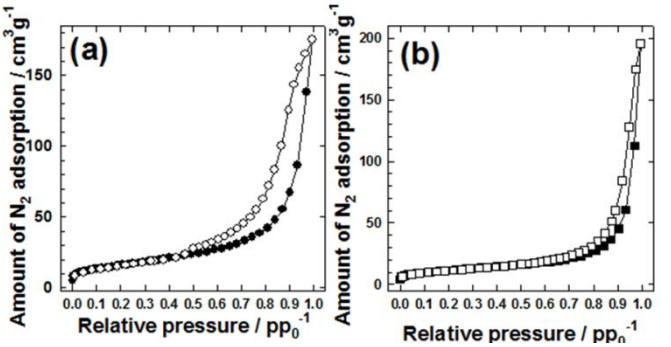

Fig. 5. N_2 adsorption–desorption isotherms of (a) **AT1** and (b) **AT2**. The close and open symbols represent the adsorption and desorption data, respectively.

Diffuse Reflectance UV–vis and PL Spectroscopy.

The diffuse reflectance UV–vis spectra of the present **AT** nanohybrids are plotted in the left panel of Fig. 6. While the pristine potassium titanoniobate shows quite large bandgap energy (E_g) of ~3.6 eV, the reference Ag_2CO_3 has much smaller bandgap energy of ~2.4 eV, clearly demonstrating its visible light harvesting ability. The hybridization of titanoniobate with silver carbonate induces the remarkable enhancement of visible light absorption, indicating the synergistic coupling between these two components.

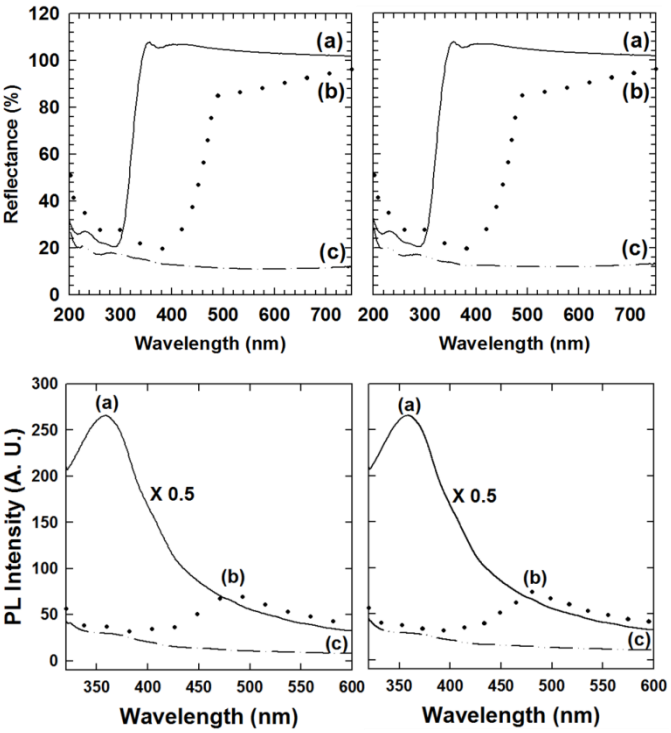

Fig. 6. (Top) Diffuse reflectance UV–vis and (bottom) PL spectra for (a) the pristine $K_3Ti_5NbO_{14}$ (solid lines), (b) Ag_2CO_3 (dotted lines), and (c) the **AT** nanohybrid (dot-dashed lines).

The curves (c) in the left and right panels represent the data of **AT1** and **AT2**, respectively.

In comparison with the unhybridized Ag_2CO_3 showing only a negligible absorptivity in the low energy region of $\lambda > 500$ nm, the present **AT** nanohybrids show much higher absorptivity in the entire region of visible light. This observation confirms the partial formation of metallic silver that can absorb the entire region of UV–vis radiation. The formation of silver metal upon the hybridization is further evidenced by the color change of titanoniobate materials from white to black, a characteristic color of elemental silver particle. Metallic Ag nanoparticle can show a plasmonic resonance absorbing visible light. However, the strong absorption of entire UV–vis region by the present **AT** nanohybrids obviously indicates the formation of Ag particle whose size is too large to induce a plasmonic resonance of nanoparticle.

The recombination between electrons and holes is an important parameter to understand the variation of photocatalytic activity, because it is closely related to the lifetime of these transient species. There are several ways of charge recombination such as radiative recombination and non-radiative recombination including Auger recombination and Shockley-Read-Hall recombination.[41] However, the contribution of the radiative recombination is important in probing the lifetime of photogenerated electrons and holes, and the variation of photocatalytic activity upon the hybridization.[41] Thus, the recombination between electrons and holes in the present nanohybrids is examined by monitoring the variation of photoluminescence (PL) signal upon the hybridization, as done in many other reports. The PL spectra of the **AT** nanohybrids are plotted in the right panel of Fig. 6, as compared with those of the precursor titanoniobate and silver carbonate. Both of the present nanohybrids display much weaker PL intensity, underscoring the depression of the charge recombination upon the hybridization. Even though the **AT2** nanohybrid possesses a larger content of Ag metal than does the **AT1** nanohybrid (see Table S1 in *Supporting Information*), there is no clear difference in the PL signals of both the materials, indicating the negligible contribution of Ag metal in the internal charge transfer of the present **AT** nanohybrids. Taking into account the relative band positions of titanoniobate and silver carbonate (see *Supporting Information*), photoinduced holes in the valence band (VB) of Ag_2CO_3 can be transferred into the upper-lying VB of Ti_5NbO_{14}, leading to the spatial separation of electrons and holes, and the increase of their lifetimes.

Ag 3d XPS Analysis.

Quantitative information about the oxidation state of silver species in the present **AT** nanohybrids is investigated with Ag 3d X-ray photoelectron spectroscopy (XPS) analysis. As plotted in Fig. 7, the references Ag metal and Ag_2CO_3 show twin XPS peaks corresponding to Ag $3d_{5/2}$ and Ag $3d_{3/2}$ states at ~368 and ~374 eV, respectively. In contrast to the XPS spectra of all the other elements, that of Ag element demonstrates a unique opposite trend of the energy shift for the variation of oxidation state; an increase of Ag oxidation state leads to the decrease of binding energy (BE). In fact, as shown in Fig. 7, the Ag_2CO_3 reference with the Ag^+ oxidation state shows a lower BE of 367.7 eV than does the neutral Ag^0 reference (BE = 368.2 eV). This is interpreted as a result of the formation of strong covalent bond between Ag^+ cation and ligand.[42] In comparison with these references, the **AT** nanohybrids display rather broader XPS peaks, suggesting the mixed presence of two kinds of silver species. According to the peak convolution analysis (see *Supporting Information*), the observed XPS spectra of the present **AT** nanohybrids are well-reproduced with the summation of the spectra of Ag_2CO_3 and Ag metal, confirming the co-existence of these two phases. The ratio of Ag metal/Ag_2CO_3 is determined to be 0.38 and 0.50 for the **AT1** and **AT2** nanohybrids, suggesting an increase of the relative concentration of neutral Ag^0 component upon the increase of Ag content in the nanohybrids.

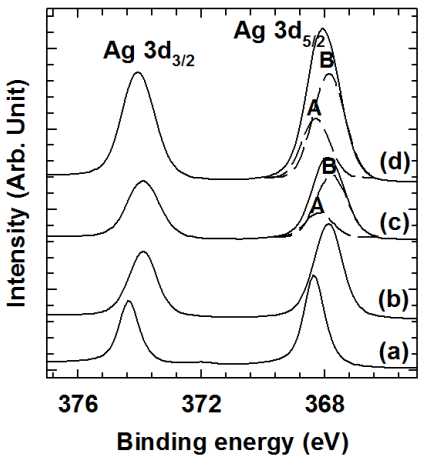

Fig. 7. Ag 3d XPS spectra of (a) Ag metal, (b) Ag_2CO_3, (c) **AT1** and (d) **AT2**.

Ag K-, Ti K-, and Nb K-Edge XANES Analyses.

The chemical bonding natures of the present **AT** nanohybrids are investigated with X-ray absorption near-edge structure (XANES) analyses at Ag K-, Ti K-, and Nb K-edges. The Ag K-edge XANES spectra of the **AT** nanohybrids are presented in the top-left panel of Fig. 8, as compared with those of the references Ag metal and Ag_2CO_3. While silver carbonate displays a strong resonance peak A corresponding to the dipole-allowed transition from 1s orbital to 5p orbital, two strong peaks A and B are discernible at higher positions for the reference Ag metal. The overall spectral features of the present **AT** nanohybrids are almost identical to that of Ag_2CO_3 not to that of Ag metal. This observation strongly suggests that, despite a strong absorption of visible light region by the **AT** nanohybrids, most of silver species in these materials exist in the form of silver carbonate and hence only a small proportion of silver cations are reduced to silver metal. This is in good agreement with the result of XPS convolution analysis.

The top-right panel of Fig. 8 represents the Ti K-edge XANES spectra of the present **AT** nanohybrids as well as the reference spectra of $K_3Ti_5NbO_{14}$, rutile TiO_2, and anatase TiO_2. All the materials under investigation demonstrate characteristic pre-edge peaks P_1, P_2, and P_3, corresponding to the transitions from core 1s level to unoccupied 3d states.[43] The spectral features of these pre-edge peaks can reflect sensitively the local atomic arrangement and oxidation state of titanium ion.[43] The obtained **AT** nanohybrids display nearly the same pre-edge spectral features as the reference $K_3Ti_5NbO_{14}$, which is clearly distinguishable from those of anatase and rutile TiO_2. This finding provides strong evidence for the maintenance of the original layered structure of titanoniobate nanosheets upon the hybridization process. In the main-edge region, the present **AT** compounds exhibit three features A, B, and C related to the

dipole-allowed 1s → 4p transitions.[43] The main-edge spectral features of the **AT** nanohybrids are almost identical to that of the pristine layered titanoniobate, indicating the negligible influence of hybridization on the local structure of titanoniobate nanosheets.

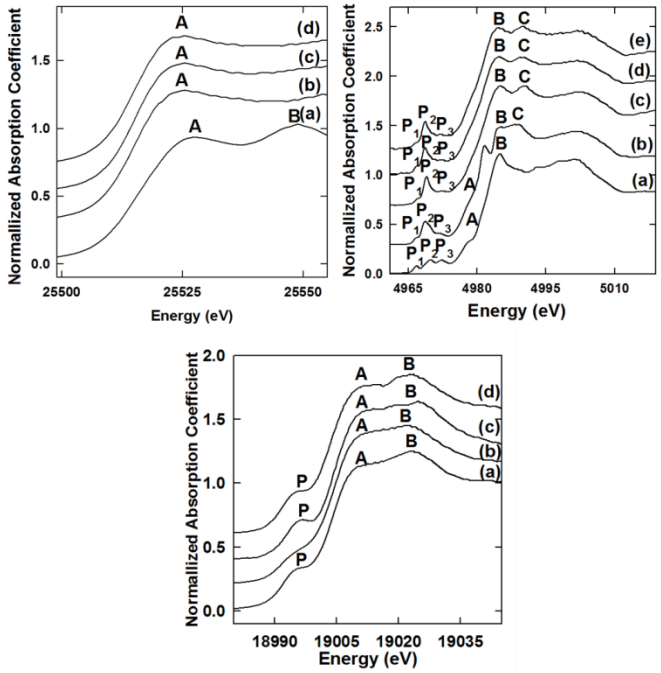

Fig. 8. (Top-left) Ag K-edge XANES spectra of (a) Ag metal, (b) Ag_2CO_3, (c) **AT1**, and (d) **AT2**. (Top-right) Ti K-edge XANES spectra for (a) anatase TiO_2, (b) rutile TiO_2, (c) the pristine $K_3Ti_5NbO_{14}$, (d) **AT1**, and (e) **AT2**. (Bottom) Nb K-edge XANES spectra for (a) the pristine $K_3Ti_5NbO_{14}$, (b) Nb_2O_5, (c) **AT1**, and (d) **AT2**.

The Nb K-edge XANES spectra of the **AT1** and **AT2** nanohybrids are presented in the bottom panel of Fig. 8, as compared with those of the pristine $K_3Ti_5NbO_{14}$ and Nb_2O_5. While the layer-structured $K_3Ti_5NbO_{14}$ reference displays a distinct pre-edge peak P, this peak does not appear in the reference spectrum of Nb_2O_5. This peak can be an indicator for the maintenance of layered titanoniobate structure. In the main-edge region, two features A and B related to the dipole-allowed 1s → 5p transitions appear for all the present **AT** compounds. There is a close spectral similarity including the peak P in the spectra of the present **AT** nanohybrids and the pristine $K_3Ti_5NbO_{14}$, confirming the retention of the original structure of titanoniobate nanosheets upon the hybridization with silver carbonate.

Summarizing all the present XANES results, the hybridized silver species exist mainly in the form of carbonate and the exfoliated titanoniobate nanosheets are successfully incorporated in the present **AT** nanohybrids without significant change in the oxidation state and local symmetry of the component metal ions. Thus, the absence of titanoniobate-related Bragg reflections in the powder XRD patterns of the **AT** nanohybrids can be understood as a result of the homogeneous dispersion of the Ti_5NbO_{14} nanosheets, instead of no incorporation of these nanosheets.

Photocatalytic Activity Test.

The photocatalytic activity of the present **AT** nanohybrids is tested for the photodegradation of 4-chlorophenol (4-CP) under the irradiation of visible light, in comparison with those of the references $K_3Ti_5NbO_{14}$ and Ag_2CO_3. In this study, transparent 4-CP molecule is selected as substrate for the test of visible light photocatalytic activity to avoid the interference of self-sensitization effect of visible light absorbing dye molecules. As presented in Fig. 9, the pristine $K_3Ti_5NbO_{14}$ is inactive for the visible light-induced photodecomposition of 4-CP, which is attributable to its large bandgap energy. Conversely, the reference Ag_2CO_3 induces the effective photocatalytic degradation of 4-CP under visible light illumination. In comparison with the unhybridized Ag_2CO_3, both the **AT** nanohybrids show higher photocatalytic activity, highlighting the usefulness of the hybridization with metal oxide nanosheet in improving the photocatalytic activity of silver oxosalts. Taking into account the wide bandgap energy of titanoniobate, the observed visible light photocatalytic activity of the present **AT** nanohybrid can be understood as a role of silver carbonate as a visible light sensitizer. As illustrated in schematic model of band structure (see *Supporting Information*), the visible light can be absorbed by the silver carbonate component and the created holes are transferred into titanoniobate species. Thus the decomposition of 4-CP molecule can occur on the surface of titanoniobate with photogenerated holes.

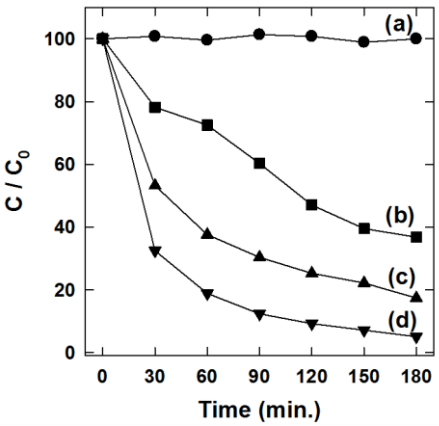

Fig. 9. Time profiles of photocatalytic degradation of 4-CP by (a) the pristine $K_3Ti_5NbO_{14}$, (b) Ag_2CO_3, (c) **AT1**, and (d) **AT2** under the irradiation of visible light ($\lambda > 420$ nm).

Between the present **AT** nanohybrids, the **AT2** nanohybrid with a smaller surface area shows a higher photocatalytic activity than does the **AT1** material, underscoring the role of silver carbonate as a visible light harvesting sensitizer. However, a further increase of Ag_2CO_3 content from the composition of the **AT2** material (i.e. Ag_2CO_3/Ti_5NbO_{14} = 1.5) leads to the lowering of the photocatalytic activity (not shown here), suggests a crucial role of layered titanoniobate nanosheet in optimizing the photocatalyst performance of silver carbonate. Since the titanoniobate nanosheet accepts holes from the hybridized silver carbonate, resulting in the extension of the lifetime of electrons and holes, and the improvement of photocatalytic activity. Thus, both the components of silver carbonate and titanoniobate are commonly important in optimizing the photocatalytic activity of the resulting

nanohybrid. Since many silver oxosalts are not stable for photocorrosion, the effect of hybridization on the photostability of silver carbonate is probed by carrying out three successive photocatalyst test for visible light (λ > 420 nm)-induced degradation of 4-CP molecule (see *Supporting Information*). The depression of photocatalytic activity is much weaker for the **AT2** nanohybrid (~84% retention after the 3rd cycle) than for Ag_2CO_3 (~45% retention after the 3rd cycle), confirming the positive effect of hybridization on the photostability of silver carbonate.

The effect of photocatalyst test on the crystal structure of the **AT2** nanohybrid is examined with powder XRD and FE-SEM analysis. As illustrated in Fig. 10, this nanohybrid retains its original crystal structure upon the photocatalytic reaction, indicating the high structural stability of the present nanohybrid material. There is a slight increase of the XRD peak of Ag metal after the photocatalyst test, indicating that the silver particles remain stable during the photoreaction and moreover a fraction of Ag_2CO_3 is reduced to Ag metal. Also the photocatalytic reaction has negligible influence on the porous morphology of the present nanohybrid, underscoring the good morphological stability of the present hybrid material. This is confirmed by the N_2 adsorption–desorption isotherm analysis showing the negligible change of surface area upon the photocatalyst test (see *Supporting Information*). The effect of photoreaction on the chemical bonding nature of silver species is also examined with Ag 3d XPS analysis for the **AT2** nanohybrid subjected to the photocatalyst test (see *Supporting Information*). There is only a weak increase of Ag^0 content after the photoreaction, clearly demonstrating the negligible variation of the chemical nature of silver species (Ag_2CO_3 and Ag metal) in the present nanohybrid.

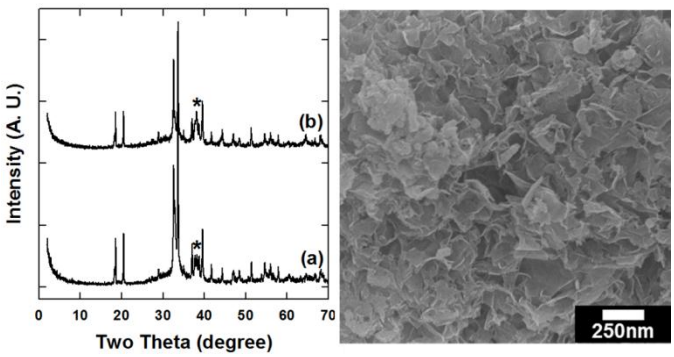

Fig. 10. (Left) Powder XRD patterns and (right) FE-SEM image of the **AT2** nanohybrid (a) before and (b) after the photocatalyst test under visible light irradiation (λ > 420 nm). The asterisk denotes the (111) Bragg reflection of Ag metal.

Experimental

Preparation

Layered potassium titanoniobate, $K_3Ti_5NbO_{14}$, was prepared by solid-state reaction and its protonated derivative was obtained the HCl treatment, respectively.[44–46] The exfoliation of layered titanoniobate was achieved by the reaction of the protonated titanoniobate with TBA·OH, leading to the formation of stable colloidal suspension of exfoliated nanosheets. The resulting colloidal suspension showed negative zeta potential of –44 mV, indicating the negatively-charged state of titanoniobate nanosheets. The hybridization between layered titanoniobate nanosheets and silver species was accomplished by the dropwise addition of the aqueous solution of silver nitrate into the colloidal suspension of exfoliated titanoniobate nanosheets at a high pH condition of ~10, leading to the crystal growth of silver carbonate/silver on the surface of the titanoniobate nanosheets, as illustrated in Fig. 2. The electrostatic interaction between anionic titanoniobate nanosheets and silver cations was responsible for the effective immobilization of silver species on the surface of titanoniobate nanosheets. The reaction was carried out at 25 °C for 24 h. The resultant precipitates were centrifuged, washed thoroughly with distilled water, and dried in oven.

Characterization

The crystal structures of the pristine layered titanoniobate and its nanohybrids were examined with powder XRD analysis (Rigaku, λ = 1.5418 Å, 298 K). The crystal morphology of the present materials was studied with FE-SEM analysis using a Jeol JSM-6700F electron microscope. The spatial elemental distribution of the obtained nanohybrids was investigated with EDS–elemental mapping analysis using an energy dispersive X-ray spectrometer equipped in FE-SEM machine. The composite structure of the **AT** nanohybrids was studied with HR-TEM analysis using a Jeol JEM-2100F microscope at an accelerating voltage of 200 kV. The pore structure and surface area of the present materials were studied by measuring volumetrically N_2 adsorption–desorption isotherms at liquid nitrogen temperature. The calcined samples were degassed at 150 °C for 2 h under vacuum before the adsorption measurement. The optical property of the nanohybrids was probed with diffuse reflectance UV–vis spectroscopy using a Perkin-Elmer Lambda 35 spectrometer equipped with an integrating sphere and PL spectroscopy using Perkin-Elmer LS55 fluorescence spectrometer. XAS experiments were carried out at the Ag K-, Ti K-, and Nb K-edge with the extended X-ray absorption fine structure (EXAFS) facility with a Si(111) single crystal monochromator installed at the beam line 10C at the Pohang Accelerator Laboratory (PAL) in Korea. All the present data were measured from the thin layer of powder samples deposited on transparent adhesive tapes in a transmission mode using gas-ionization detectors. The energy of all the present spectra was carefully referenced to the simultaneously-measured spectra of metal foil. The present XPS spectra were measured for a thin layer of the sample on highly conductive copper foil using XPS spectrometer with a twin source of X-ray beams, resulting in the depression of the charging effect. All the XPS spectra were calibrated on the basis of the adventitious C 1s peak at 284.8 eV to rule out the spectral modification by the charging effect.

Photocatalytic Reactivity Test

The photocatalytic activity of the present materials was tested for the photodegradation of 4-CP under the illumination of visible light (λ > 420 nm). The 4-CP substrate was added to an aqueous photocatalyst suspension in the glass reactor (40 mL) with a quartz window and then equilibrated for 1 h with stirring in the dark before illumination. Light from a 300-W Xe arc lamp (Oriel) was passed through a 10-cm IR water filter and a cutoff filter (λ > 420 nm) to eliminate IR and UV radiations, respectively. Sample aliquots were drawn by a 1-mL syringe intermittently during the photoreaction and filtered through a 0.45-μm PTFE filter (Milipore) to remove catalyst particles. To rule out the effect of the adsorption of substrate on the

surface of catalyst, the variation of substrate concentration was measured after the equilibration under dark condition. The concentration of 4-CP was estimated with a reverse-phase high performance liquid chromatograph (HPLC, Agilent 1100 series). The eluent solution was composed of acetonitrile (40%) and deionized water (60%). After the photoreaction, the photocatalysts were restored by centrifugation to probe the evolution of their crystal structure and morphology with XRD and FE-SEM analyses.

Conclusions

In the present work, we develop a novel facile and efficient method to hybridize Ag_2CO_3/Ag with semiconducting metal oxide. The obtained Ag_2CO_3/Ag–layered Ti_5NbO_{14} nanohybrids display much superior visible light photocatalytic activity compared with the unhybridized Ag_2CO_3, highlighting the remarkable enhancement of the photocatalytic activity of silver oxosalt upon hybridization. In this nanohybrid system, the silver carbonate acts as a visible light absorbing sensitizer whereas the titanoniobate nanosheet plays a role of a scaffold to form highly porous structure and a hole acceptor to induce the extension of the lifetimes of electrons and holes. The present results clearly demonstrate the usefulness of the exfoliation–crystal growth method in exploring new efficient hybrid photocatalyst materials. Taking into account the facile crystal growth of silver oxosalts in aqueous media, the present synthetic method is readily applicable for other couples of silver oxosalts and inorganic nanosheets. Currently we are trying to synthesize new type of visible light photocatalysts by the incorporation of silver oxosalts into the 3D porous structures of metal oxide photocatalysts.

Acknowledgements

This research is supported by the Core Technology of Materials Research and Development Program of the Korea Ministry of Intelligence and Economy (grant No. 10041232) and by Korea Ministry of Environment as "Converging Technology Project" (191-101-001). The experiments at PAL were supported in part by MOST and POSTECH.

Notes and references

[a]Department of Chemistry and Nano Sciences, Ewha Womans University, Seoul 120-750, Korea. Fax: +82-2-3277-3419; Tel: +82-2-3277-4370; E-mail: hwangsju@ewha.ac.kr

† These two authors contributed equally to this work.

† Electronic Supplementary Information (ESI) available: [XPS fitting results, band structure model, and the results of successive photocatalyst tests for **AT** nanohybrid, N_2 adsorption–desorption isotherm and XPS data of **AT** nanohybrid and Ag_2CO_3 subjected to the photocatalyst test]. See DOI: 10.1039/b000000x/

1 A. Fujishima and K. Honda, *Nature*, 1972, **238**, 37.
2 N. Zeug, J. Buecheler and H. Kisch, *J. Am. Chem. Soc.*, 1985, **107**, 1459.
3 L. Huang, H. Xu, Y. Li, H. Li, X. Cheng, J. Xia, Y. Xua and G. Caia, *Dalton Trans*., 2013, **42**, 8606.
4 Z. Zou, J. Ye, K. Sayama and H. Arakawa, *Nature*, 2001, **414**, 625.
5 D. E. Zhang, J. Y. Gong, J. J. Ma, G. Q. Hana and Z. W. Tong, *Dalton Trans*., 2013, **42**, 16556.
6 H. Kato, K. Asakura and A. Kudo, *J. Am. Chem. Soc.*, 2003, **125**, 3082.
7 S. Wang, H. Qian, Y. Hu, W. Dai, Y. Zhong, J. Chen and X. Hu, *Dalton Trans*., 2013, **42**, 1122.
8 N. S. Lewis and D. G. Nocera, *Proc. Natl. Acad. Sci. U.S.A.*, 2006, **103**, 15729.
9 A. Kudo and Y. Miseki, *Chem. Soc. Rev.*, 2009, **38**, 253.
10 Y. Ni, Y. Zhu and X. Ma, *Dalton Trans*., 2011, **40**, 3689.
11 H. Zhou, X. Li, T. Fan, F. E. Osterloh, J. Ding, E. M. Sabio, D. Zhang and Q. Guo, *Adv. Mater.*, 2010, **22**, 951.
12 H. N. Kim, T. W. Kim, I. Y. Kim and S. -J. Hwang, *Adv. Funct. Mater*., 2011, **21**, 3111.
13 T. Hirai, H. Okubo and I. Komasawa, *J. Colloid Interf. Sci.*, 2001, **235**, 358.
14 J. H. Wu, J. M. Lin, Y. B. Shu and T. J. Sato, *J. Mater. Chem.*, 2001, **11**, 3343.
15 W. F. Shangguan and A. Yoshida, *Sol. Energy Mater. Sol. Cells*, 2001, **69**, 189.
16 W. F. Shangguan and A. Yoshida, *J. Phys. Chem. B*, 2002, **106**, 12227.
17 J. L. Gunjakar, T. W. Kim, H. N. Kim, I. Y. Kim and S. -J. Hwang, *J. Am. Chem. Soc.*, 2011, **133**, 14998.
18 T. W. Kim, S. -J. Hwang, Y. Park, W. Choi and J. -H. Choy, *J. Phys. Chem. C*, 2007, **111**, 1658.
19 T. W. Kim, M. J. Paek, H. W. Ha, S. H. Hyun, J. -H. Choy and S. -J. Hwang, *J. Mater. Chem.*, 2010, **20**, 3238.
20 T. W. Kim, H. W. Ha, M. J. Paek, I. H. Paek, S. H. Hyun, J. -H. Choy and S. -J. Hwang, *J. Phys. Chem. C*, 2008, **112**, 14853.
21 T. W. Kim, S. -J. Hwang, S. H. Jhung, J. S. Chang, H. Park, W. Choi and J. -H. Choy, *Adv. Mater*., 2008, **20**, 539.
22 T. W. Kim, S. G. Hur, S. -J. Hwang and J. -H. Choy, *Chem. Commun.*, 2006, 220.
23 T. W. Kim, S. G. Hur, S. -J. Hwang, H. Park, W. Choi and J. -H. Choy, *Adv. Funct. Mater.*, 2007, **17**, 307.
24 M. J. Paek, T. W. Kim and S. -J. Hwang, *J. Phys. Chem. Solids*, 2008, **69**, 1444.
25 T. W. Kim, E. -J. Oh, A. Y. Jee, S. T. Lim, D. H. Park, M. Lee, S. -H. Hyun, J. -H. Choy and S. -J. Hwang, *Chem. Eur. J.*, 2009, ***15***, 10752.
26 S. M. Paek, J. H. Kang, H. Jung, S. -J. Hwang and J. -H. Choy, *Chem. Commun*., 2009, 7536.
27 Y. R. Lee, M. A Woo, K. M. Lee, T. W. Kim, J. -H. Choy and S. -J. Hwang, *J. Phys. Chem. Solids*, 2012, **73**, 1492.
28 E. J. Oh, T. W. Kim, K. M. Lee, M. S. Song, A. Y. Jee, S. T. Lim, H. W. Ha, M. Lee, J. -H. Choy and S. -J. Hwang, *ACS Nano*, 2010, **4**, 4437.
29 K. Akatsuka, M. A. Haga, Y. Ebina, M. Osada, K. Fukuda and T. Sasaki, *ACS Nano*, 2009, **3**, 1097.
30 L. Wang, Y. Ebina, K. Takada and T. Sasaki, *J. Phys. Chem. B*, 2004, **108**, 4283.
31 I. Y. Kim, J. M. Lee, T. W. Kim, H. N. Kim, H. Kim, W. Choi and S. -J. Hwang, *Small*, 2012, **8**, 1038.
32 M. S. Song, K. M. Lee, Y. R. Lee, I. Y. Kim, T. W. Kim, J. L. Gunjakar and S. -J. Hwang, *J. Phys. Chem. C*, 2010, **114**, 22134.
33 G. Dai, J. Yu and G. Liu, *J. Phys. Chem. C*, 2012, **116**, 15519.
34 Y. K. Jo, I. Y. Kim, J. M. Lee, S. Nahm, J. -Y. Choi and S. -J. Hwang, *Mater. Lett.*, 2014, **114**, 152.

35 C. Xu, Y. Liu, B. Huang, H. Li, X. Qin, X. Zhang and Y. Dai, *J. Mater. Chem. A*, 2011, **257**, 8732.
36 S. Kumar, T. Surendar, A. Baruah and V. Shanker, *J. Mater. Chem. A*, 2013, **1**, 5333.
37 Q. Liang, Y. Shi, W. Ma, Z. Li and X. Yang, *Phys. Chem. Chem. Phys.*, 2012, **14**, 15657.
38 J. Yan, Z. Fan, T. Wei, W. Qian, M. Zhang and F. Wei, *Carbon*, 2010, **48**, 3825.
39 S. J. Gregg and K. S. W. Sing, *Academic Press*, London, 1976.
40 P, Yuan, H. He, F. Bergaya, D. Wu, Q. Zhou and J. Zhu, *Micropor. Mesopor. Mater*., 2006, **88**, 8.
41 J. Liqiang, Q. Yichun, W. Baiqi, L. Shudan, J. Baojiang, Y. Libin, F. Wei, F. Honggang and S. Jiashong, *Solar Energy Mater. Solar Cells*, 2006, **90**, 1773
42 S. W. Gaarenstroom and N. Winograd, *J. Chem. Phys.*, 1977, **67**, 15.
43 S. G. Hur, D. H. Park, T. W. Kim and S. -J. Hwang, *Appl. Phys. Lett.*, 2004, **85**, 4130.
44 K. Domen, Y. Ebina, S. Ikeda, A. Tanaka, J. N. Kondo and K. Maruya, *Catal. Today*, 1996, **28**, 167.
45 A. Takagaki, T. Yoshida, D. Lu, J. N. Kondo, M. Hara, K. Domen and S. Hayashi, *J. Phys. Chem. B*, 2004, **108**, 11549.
46 M. Hervieu, H. Rebbah, G. Desgardin and B. Raveau, *J. Solid State Chem.*, 1980, **35**, 200.

A Graphic Abstract for **"A Facile Exfoliation–Crystal Growth Route to Multicomponent Ag_2CO_3/Ag–Ti_5NbO_{14} Nanohybrids with Improved Visible Light Photocatalytic Activity"**

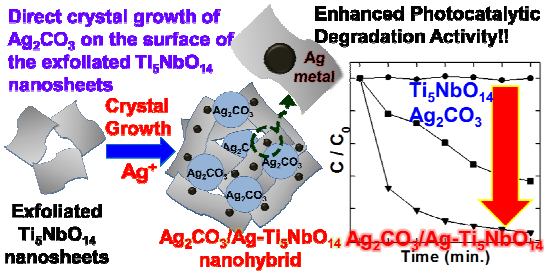

: Novel visible light active photocatalyst is developed via a direct crystal growth of silver oxosalt on exfoliated titanoniobate nanosheet.